3 Mass Sensitivity in e^+e^-

To illustrate the mass sensitivity of our observable, we begin with the simplest case of e^+e^- collisions. We simulate the $e^+e^- \to t + X$ process at a center of mass energy of $Q = 2000$ GeV using the PYTHIA8 parton shower and reconstruct anti-k_T jets with $R = 1.2$. Although jet clustering is not required in e^+e^-, this analysis strategy is chosen to achieve maximal similarity with the case of hadron colliders.

In the left panel of Fig. 1 we show the distribution of the three-point correlator in the peak region, both with and without the effects of hadronization. Agreement of the peak position with the leading-order expectation is found, showing that the observed behavior is dictated by the hard decay of the top. In Fig. 1, linear ($n = 1$) and quadratic ($n = 2$) energy weightings are used, see Eq. (2). The latter is not collinear safe, but the collinear IR-divergences can be absorbed into moments of the fragmentation functions or track functions.

Crucially, non-perturbative effects in energy correlators are governed by an additive underlying power law [19, 9], which over the width of the peak has a minimal effect on the normalized distribution. This is confirmed by the small differences in peak position between parton and hadron level distributions in Fig. 1. Taking $m_t = 170, 172$ GeV with $n = 2$ as representative distributions, we find that the shift due to hadronization corresponds to a $\Delta m_t^{\text{Had.}} \sim 250$ MeV shift in m_t. This is in contrast with the groomed jet mass case where hadronization causes peak shifts equivalent to $\Delta m_t^{\text{Had.}} \sim 1$ GeV [20].

4 Hadron Colliders

We now extend our discussion to the more challenging case of proton-proton collisions. This study illustrates the difference between energy correlators and standard jet shape observables, and also emphasizes the irreducible difficulties of jet substructure at hadron colliders.

At variance with the case of e^+e^- annihilations, the hadronic final states in proton-proton collisions on which the energy correlators are computed are necessarily defined through a measurement, e.g. by selecting anti-k_T jets with a specific $p_{T,\text{jet}}$. Due to the insensitivity of the energy correlators to soft radiation, it is in fact the non-perturbative effects on the jet p_T selection that are the only source of complications in a hadron collider environment [14]. This represents a significant advantage of our approach, since it shifts the standard problem of characterizing non-perturbative corrections to infrared jet shape observables, to characterizing non-perturbative effects on a *hard* scale. This enables us to propose a methodology for the precise extraction of m_t in hadron collisions by independently measuring the universal non-perturbative effects on the $p_{T,\text{jet}}$ spectrum. We now illustrate the key features of this approach.

The three-point correlator in hadron collisions is defined as

$$\widehat{\mathcal{M}}^{(n)}_{(pp)}(\zeta_{12},\zeta_{23},\zeta_{31}) = \sum_{i,j,k\,\in\,\text{jet}} \frac{(p_{T,i})^n (p_{T,j})^n (p_{T,k})^n}{(p_{T,\text{jet}})^{3n}} \delta\left(\zeta_{12} - \hat{\zeta}^{(pp)}_{ij}\right) \delta\left(\zeta_{23} - \hat{\zeta}^{(pp)}_{ik}\right) \delta\left(\zeta_{31} - \hat{\zeta}^{(pp)}_{jk}\right), \quad (6)$$

where $\hat{\zeta}^{(pp)}_{ij} = \Delta R^2_{ij} = \sqrt{\Delta\eta^2_{ij} + \Delta\phi^2_{ij}}$, with η, ϕ the standard rapidity, azimuth coordinates.

The peak of the EEEC distribution is determined by the hard kinematics and is found at $\zeta^{(pp)}_{\text{peak}} \approx 3m_t^2/p^2_{T,t}$, where $p_{T,t}$ is the hard top p_T, *not* $p_{T,\text{jet}}$.

To clearly illustrate the distinction between the infrared measurement of the EEEC and the hard measurement of the $p_{T,\text{jet}}$ spectrum, we present a two-step analysis using data generated in PYTHIA8 [14]. First, we generated hard top quark states with definite momentum (like in e^+e^-), but in the more complicated LHC environment including the underlying event (UE). This is shown in the right panel of

Fig. 1, where we see a clear peak that is *completely* independent of the presence of MPI (the PYTHIA8 model for UE), which illustrates that the correlators themselves, on a perfectly characterized top quark state, are insensitive to soft radiation *without* grooming.

In ref. [14] a proof-of-principles analysis was performed to illustrate that a characterization of non-perturbative corrections to the $p_{T,\text{jet}}$ spectrum allows us to extract m_t, with small uncertainties from non-perturbative physics. To extract a value of m_t, we write the peak position as

$$\zeta^{(pp)}_{\text{peak}} = \frac{3F_{\text{pert}}(m_t, p_{T,\text{jet}}, \alpha_s, R)}{\left(p_{T,\text{jet}} + \Delta_{\text{NP}}(R) + \Delta_{\text{MPI}}(R)\right)^2}\,, \tag{7}$$

where F_{pert} incorporates the effects of perturbative radiation. At leading order, $F_{\text{pert}} = m_t^2$. Corrections from hadronization and MPI are encoded through the shifts $\Delta_{\text{NP}}(R)$ and $\Delta_{\text{MPI}}(R)$. Crucially, in the factorization limit that we consider, these are not a property of the EEEC observable, but can instead be extracted directly from the non-perturbative corrections to the jet p_T spectrum [21]. This is a unique feature of our approach.

The next step would be to calculate F_{pert} at NLO in perturbative QCD within a well-defined short-distance top mass scheme (such as the MSR [22]) and use the result to extract m_t according to the procedure described below. However, since the computation of F_{pert} has not been performed yet, in order to illustrate the feasibility of our approach, we have used PYTHIA8 (including hadronization and MPI) to extract $\zeta^{(pp)}_{\text{peak}}$ as a function of $p_{T,\text{jet}}$, over an energy range within the expected reach of the high luminosity LHC. As a proxy for the perturbative calculation, we used parton-level simulations to extract F_{pert}. To the accuracy we are working, F_{pert} is independent of the jet p_T, and can just be viewed as an effective top mass $\sqrt{F_{\text{pert}}}(m_t)$. We also extract $\Delta_{\text{NP}}(R) + \Delta_{\text{MPI}}(R)$ independently from the $p_{T,\text{jet}}$ spectrum.

Using Eq. (7) we fit $\zeta^{(pp)}_{\text{peak}}$ as a function of $p_{T,\text{jet}}$ for an effective value of $F_{\text{pert}}(m_t)$. With a perfect characterization of the non-perturbative corrections to the EEEC observable, the value of $F_{\text{pert}}(m_t)$ extracted when hadronization and MPI are included should exactly match its extraction at parton level. This would lead to complete control over m_t. In Table 1 we show the extracted value of $F_{\text{pert}}(m_t)$ from our parton level fit, and from our hadron+MPI level fit for two values of the PYTHIA8 m_t. The errors quoted are the statistical errors on the parton shower analysis. The Hadron+MPI fit is quoted with two errors: the first originates from the statistical error on the EEEC measurement, the second stems from the statistical error on the determination of $\Delta_{\text{NP}}(R) + \Delta_{\text{MPI}}(R)$ from the $p_{T,\text{jet}}$ spectrum. A more detailed discussion of this procedure can be found in the *Supplemental Material* in [14]. Thus we find promising evidence that theoretical control of m_t, with conservative errors $\lesssim 1$GeV, is possible with an EEEC-based measurement. We stress that systematically improvable calculations of $F_{\text{pert}}(m_t)$ within our approach are made feasible by a factorization formula for the weighted cross section discussed in ref. [14]. Theory errors are contingent upon currently unavailable NLO computations, see the discussion in [14]. However, we expect observable-dependent NLO theory errors on m_t to be better than those in other inclusive measurements wherein in the dominant theory errors are from PDFs+α_s [23, 24] and which mostly affect the normalization of the observable. By contrast the EEEC is also inclusive but the extracted m_t is only sensitive to the observable's shape.

Our promising results motivate developing a deeper theoretical understanding of the three-point correlator of boosted tops in the hadron collider environment. Nevertheless, there remain many areas in which our methodology could be improved to achieve greater statistical power and bring it closer to experimental reality. These include the optimization of $\delta\zeta$, the binning of $p_{T,\text{jet}}$ and $\zeta^{(pp)}$, and including other shapes on the EEEC correlator. Regardless, our analysis does demonstrate the observable's potential for

PYTHIA8 m_t	Parton $\sqrt{F_{\rm pert}}$	Hadron + MPI $\sqrt{F_{\rm pert}}$
172 GeV	172.6 ± 0.3 GeV	$172.3 \pm 0.2 \pm 0.4$ GeV
173 GeV	173.5 ± 0.3 GeV	$173.6 \pm 0.2 \pm 0.4$ GeV
175 GeV	175.5 ± 0.4 GeV	$175.1 \pm 0.3 \pm 0.4$ GeV
$173 - 172$	0.9 ± 0.4 GeV	1.3 ± 0.6 GeV
$175 - 172$	2.9 ± 0.5 GeV	2.8 ± 0.6 GeV

Table 1: The effective parameter $F_{\rm pert}(m_t)$ extracted at parton level, and hadron+MPI level. The consistency of the two simulations provides a measure of our uncertainty due to uncontrolled non-perturbative corrections. Statistical errors are shown.

a precision m_t extraction when measured on a sufficiently large sample of boosted tops. We are optimistic that such a sample will be accessible at the HL-LHC where it is forecast that $\sim 10^7$ boosted top events with $p_T > 500\,\text{GeV}$ will be measured [25]. Our results support the possibility of achieving complete theoretical control over an observable with top mass sensitivity competitive with direct measurements whilst avoiding the ambiguities associated with the usage of MC event generators.

References

1. G. Corcella, Front. in Phys. **7**, 54 (2019).
2. A.H. Hoang, Ann. Rev. Nucl. Part. Sci. **70**, 225 (2020).
3. A.H. Hoang, S. Mantry, A. Pathak and I.W. Stewart, JHEP **12**, 002 (2019).
4. J. Kieseler, K. Lipka and S.-O. Moch, Phys. Rev. Lett. **116**, 162001 (2016).
5. M. Butenschoen, B. Denhadi, A.H. Hoang, V. Mateu, M. Preisser and I.W. Stewart, Phys. Rev. Lett. **117**, 232001 (2016).
6. A.H. Hoang, S. Plätzer and D. Samitz, JHEP **10**, 200 (2018).
7. H. Chen, I. Moult, X.Y. Zhang and H.X. Zhu, Phys. Rev. D **5**, 054012 (2020).
8. N.A. Sveshnikov and F.V. Tkachov, Phys. Lett. B **382**, 403 (1996).
9. G.P. Korchemsky and G.F. Sterman, Nucl. Phys. B **555**, 335 (1999).
10. D. Hofman and J. Maldacena, JHEP **05**, 012 (2008).
11. C.L. Basham, L.S. Brown, S.D. Ellis and S.T. Love, Phys. Rev. Lett. **41**, 1585 (1978).
12. Y. Li, I. Moult, S. Schrijnder van Velzen, W.J. Waalewijn and H.X. Zhu, Phys. Rev. Lett **18**, 182001 (2022).
13. H.-M. Chang, M. Procura, J. Thaler and W.J. Waalewijn, Phys. Rev. Lett. **111**, 102002 (2013).
14. J. Holguin, I. Moult, A. Pathak and M. Procura, arXiv:2201.08393 [hep-ph].
15. L.J. Dixon, M.-X. Luo, V. Shtabovenko, T.-Z. Yang and H.X. Zhu, Phys. Rev. Lett. **120**, 102001 (2018).
16. H. Chen, M.-X. Luo, I. Moult, T.-Z. Yang, X. Zhang and H.X. Zhu, JHEP **08**, 028 (2020).

17. M. Jankowiak and A.J. Larkoski, JHEP **06**, 057 (2011).

18. P.T. Komiske, I. Moult, J. Thaler and H.X. Zhu, arXiv:2201.07800 [hep-ph].

19. G.P. Korchemsky and G.F. Sterman, Nucl. Phys. B **437**, 415 (1995).

20. A.H. Hoang, S. Mantry, A. Pathak and I.W. Stewart, Phys. Rev. D **100**, 074021 (2019).

21. M. Dasgupta, L. Magnea and G.P. Salam, JHEP **02**, 055 (2008).

22. A.H. Hoang, A. Jain, I. Scimemi and I.W. Stewart, Phys. Rev. Lett **101**, 151602 (2008).

23. S. Chatrchyan et al., Phys. Lett. B **728**, 496 (2014).

24. A.M. Sirunyan et al., JHEP **09**, 051 (2017).

25. P. Azzi et al., CERN Yellow Rep. Monogr. **7**, 1 (2019).

Frascati Physics Series Vol. 73 (2022)
LFC22: Strong interactions from QCD to new strong dynamics at LHC and Future Colliders
August 29 - September 2, 2022

NON-FACTORISABLE CORRECTIONS TO t-CHANNEL SINGLE-TOP PRODUCTION: COMPARING RESULTS FOR THE LHC AND FCC

Christian Brønnum-Hansen
Institute for Theoretical Particle Physics, Karlsruhe Institute of Technology (KIT), Wolfgang-Gaede-Strae 1, 76131 Karlsruhe, Germany
Jérémie Quarroz
Institute for Theoretical Particle Physics, Karlsruhe Institute of Technology (KIT), Wolfgang-Gaede-Strae 1, 76131 Karlsruhe, Germany
Chiara Signorile-Signorile
Institute for Theoretical Particle Physics, Karlsruhe Institute of Technology (KIT), Wolfgang-Gaede-Strae 1, 76131 Karlsruhe, Germany, Institute for Astroparticle Physics, Karlsruhe Institute of Technology (KIT), Hermann-von-Helmholtz-Platz 1, 76344 Eggenstein-Leopoldshafen, Germany
Chen-Yu Wang
Institute for Theoretical Particle Physics, Karlsruhe Institute of Technology (KIT), Wolfgang-Gaede-Strae 1, 76131 Karlsruhe, Germany Max-Planck-Institut fr Physik, Fhringer Ring 6, 80805 Mnchen, Germany

Abstract

In this contribution we report on the recent calculation of QCD non-factorisable corrections to t-channel single-top production and stress the importance of these corrections in the light of increasing the accuracy of theoretical predictions for this process. We present results for the total cross section and for selected observables relevant for proton-proton collisions at the LHC and the FCC.

TTP23-006, P3H-23-011

1 Introduction

The large mass and the strong coupling with the Higgs boson makes the top quark a favorite candidate to improve our understanding of the Standard Model, and possibly reveal heavy new physics. A large fraction of the top quarks produced at the LHC emerges from electroweak interactions, via the so-called t-channel single-top production. Predictions for this process can be used, for instance, to constrain the CKM matrix element V_{bt}, and probe possible anomalous couplings in the tWb vertex. QCD corrections to t-channel single-top production are known up to next-to-next-to-leading order (NNLO) in the factorisable approximation [1, 2, 3, 4], namely neglecting the crosstalk between different quark lines (see the left panel of Fig.1 for an example of a Feynman diagram contributing to the factorisable corrections). Factorisable corrections are found to be considerably small and only impact the cross section at $\mathcal{O}(1\%)$. Given the current level of the theory precision, it is useful to go beyond this approximation, and compute the non-factorisable corrections (see the right panel of Fig.1 for an example of Feynman diagram). This contribution vanishes at NLO, due to colour conservation, and it is colour suppressed at NNLO by a factor $N_c^2 - 1 = 8$ with respect to the factorisable corrections. However, it has been recently argued

Table 1: *Comparison of the poles of the two-loop amplitude with the ones predicted using Catani's operator for* $s \sim 104.337\,\mathrm{GeV}^2$ *and* $t \sim -5179.68\,\mathrm{GeV}^2$.

	ϵ^{-2}	ϵ^{-1}
$\langle \mathcal{A}^{(0)} \vert \mathcal{A}^{(2)}_{\mathrm{nf}} \rangle$	$-229.0940408654660 - 8.978163333241640i$	$-301.1802988944764 - 264.1773596529505i$
Catani	$-229.0940408654665 - 8.978163333241973i$	$-301.1802988944791 - 264.1773596529535i$

that an enhancement factor π^2, due to the Glauber phase, may enhance non-factorisable corrections and compensate for the colour suppression. This effect was explicitly proven to occur in the calculation of non-factorisable corrections to the vector boson fusion in the eikonal approximation [5].
In this document we summarise the results obtained for the non-factorisable corrections to t-channel single-top production [6, 7, 8] and discuss their relevance for 13 TeV and 100 TeV proton-proton collisions.

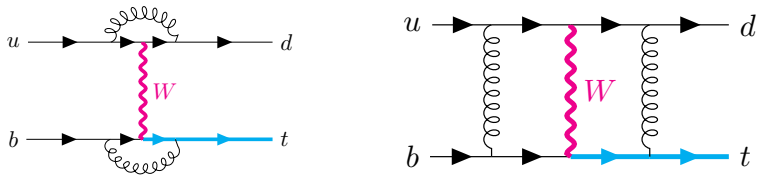

Figure 1: *Left panel: example of Feynman diagram contributing to factorisable corrections. Right panel: example of diagram contributing to non-factorisable corrections. Massless quarks are indicated with thin black line, while the massive top-quark is depicted with a blue solid line.*

2 Ingredients of the calculation

One crucial ingredient for the calculation is the double-virtual correction. In this regard, the most challenging part is the evaluation of the two-loop amplitude associated to non-factorisable diagrams as in the right panel of Fig. 1. The double-virtual amplitude is obtained numerically through the auxiliary mass flow method [10, 11]. We refer the reader to Ref. [6] for further details. Here we emphasise that the reduction of the amplitude is done analytically, retaining the full dependence on the kinematic scales s, t, m_W and m_t. The evaluation of the master integrals can be performed to any desired accuracy within a modest computing time (for a typical phase space point, 20 digits accuracy can be reached in about 30 minutes on a single core). In Tab. 2, we present the poles obtained for the two-loop amplitude compared to those predicted by Catani's operator [9]. The match between the two values degrades by only one digit per ϵ-order, starting with an agreement of 15 digits at ϵ^{-2}. We then expect a 13 digits accuracy for the finite part. To evaluate the cross section, we prepare a grid optimised for the Born cross section. We extract 10 independent sets of 10^4 points from this grid and evaluate the amplitude for each of these points. The resulting accuracy can be estimated to be $\mathcal{O}(2\%)$.

A further non-trivial element of the calculation is the evaluation of real-virtual amplitudes, and of the corresponding cross-section level contribution. The challenge is related to the presence of numerous mass scales and to the necessity of having stable results also in kinematic regions where the extra radiation becomes unresolved. We note that working with unticommuting γ_5 in d dimensions, we can calculate